A Numerical Study on Flow and Heat Transfer Characteristics of Film Cooling with a Compound Angle Hole

Jung Hee Lee* and Young Ki Choi**

(*Received October 4, 1997*)

A numerical simulation has been performed for the investigation of flow and heat transfer characteristics of a film cooling system injected through a hole with compound angle orientation. The finite volume method is employed to discretize the governing equations based on the non-orthogonal coordinate with non-staggered variable arrangement. In order to analyze flow and heat transfer characteristics, velocity, temperature, aerodynamic loss coefficient, skin friction and vorticity are calculated with the variation of the skew angle. The maximum longitudinal vorticity and aerodynamics loss depend strongly on the skew angle. For the symmetric case of $\beta=0$ deg, a pair of counter-rotating vortices are formed and the maximum value of the film cooling effectiveness has appeared in the center plane where the skin friction is the minimum. For the skew angle of $\beta=30$ deg and above, only one strong counter-clockwise vortex remains in the downstream region and the maximum value of the film cooling effectiveness are obtained on the right side of the vortex. The predicted results for the film cooling effectiveness show good agreements with previous experimental data except the near-hole region.

Key Words: Film Cooling, Finite Volume Method, Longitudinal Vortex, Film Cooling Effectiveness, Longitudinal Skin Friction, Skew Angle.

Nomenclature

C_{fX}	: Longitudinal skin friction coefficient
C_{fZ}	: Lateral skin friction coefficient
$C_{P,inj}$	: Total pressure loss coefficient measured with injection
D	: Hole diameter
$D.R.$	: Density ratio ($=\rho_j/\rho_\infty$)
k	: Turbulent kinetic energy
L	: Hole length
M	: Blowing ratio ($=\rho_j U_j/\rho_\infty U_\infty$)
P_{inj}	: Total pressure predicted with injection
P_k	: Production of the turbulent kinetic energy
Pr, Pr_t	: Laminar and turbulent Prandtl number
P_∞	: Freestream total pressure
Re_D	: Reynolds number based on the hole diameter
U_{in}, T_{in}	: Inlet velocity and temperature in the plenum region
U_j, T_j	: Jet exit velocity and temperature
U_∞, T_∞	: Freestream velocity and temperature of the main flow
X	: Coordinate in streamwise direction
Y	: Coordinate in normal direction
Z	: Coordinate in spanwise direction
α	: Inclined angle
α_m^j	: Cartesian component of the contravariant base vectors
β	: Skew angle
δ	: Boundary layer thickness
δ_n	: Normal distance from a wall
ϵ	: Dissipation rate of the turbulent kinetic energy
η	: Film cooling effectiveness
κ	: Von-Karman constant
μ, μ_t	: Laminar and turbulent viscosity

* Graduate School, Chung-Ang University, Seoul 156-756, KOREA

** Department of Mechanical Engineering, Chung-Ang University, Seoul 156-756, KOREA

ρ_j, ρ_∞ : Density of injected and mainstream fluid

σ_k, σ_ε : Turbulent diffusion Prantdl number for k and ε

Γ : Diffusion coefficient

Ω_X : Longitudinal vorticity

1. Introduction

Film cooling has been widely used for protecting the turbine blades exposed to high-temperature gas. It is a cooling method that isolates the local heat transfer by forming a protective film over the blade surface with coolant flow injected through a row of holes and lowers the average temperature in the boundary layer due to mixing of the coolant flow and mainstream. The three-dimensional nature of flow and heat transfer characteristics in the vicinity and in the downstream region depends strongly on the hole geometry, spacing, injection angles, blowing rate and density ratio. In particular, the effects of the injection angles and blowing ratio are of great importance. Most of the previous studies on flow and heat transfer characteristics were carried out experimentally for the streamwise injected jet flow.

Sinha et al. (1991) investigated the flow and heat transfer characteristics in the vicinity of a hole with the variation of the velocity ratio, density ratio and hole spacing. Near the hole, the flow and heat transfer depend strongly on the velocity ratio. Leylek and Zerkle(1994) studied the flow characteristics of the jet flow injected through a row of holes with a hole length-to-diameter ratio of $LD=3.5$ and an inclined angle of $\alpha=35$ deg. The flow fields within the hole and in the mainstream region were calculated by using the commercial PHOENICS code. The jet flow within the hole had fully three-dimensional flow characteristics, such as axisymmetric counter-rotating vortices and jetting effect.

However, most of the actual turbine blade holes have skew angle as well as inclined angle with rotation of the turbine. Flow and heat transfer characteristics with the variation of the skew angle have been recently studied. A numerical study of flow and heat transfer nature was carried out with the variation of the skew angle in range between 0 and 120 deg by Zhang and Collins (1993) using the commercial FLOW3D code. The longitudinal vortices generated by interaction between two fluids formed the region of the high longitudinal skin friction coefficient and convective heat transfer coefficient on the left side of the vortex and the region of the low longitudinal skin friction coefficient and convective heat transfer coefficient on the right side of the vortex. Lee et al. (1997) investigated the flow characteristics with the increment of the skew angle in range between 0 and 90 deg. The aerodynamic loss coefficient was increased with increment of the skew angle and the maximum vorticity was observed at the skew angle of $\beta=60$ deg. Honami et al. (1994) measured the longitudinal velocity and temperature distributions with increment of the blowing ratio at the fixed inclined angle of $\alpha=30$ deg and skew angle of $\beta=90$ deg. The maximum vorticity strongly depends on the blowing ratio. Compton and Johnston(1992) also measured the longitudinal velocity and maximum vorticity distributions with variation of the velocity ratio and skew angle in range between 0 and 180 deg to investigate the flow and heat transfer characteristics. The maximum vorticity was dependent strongly on the jet velocity and skew angle, and an optimal skew angle was obtained between 45 and 90 deg. Ligrani and Mitchell(1994) studied the effect of the longitudinal vortices in the boundary layer on the flow and heat transfer over a flat plate with the inclined and skewed hole.

In the present study, the aerodynamics loss coefficient, longitudinal vorticity and skin friction for the geometry shown in Fig. 1 were calculated

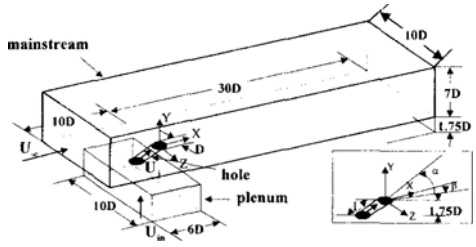

Fig. 1 Schematic diagram of the test geometry.

numerically with the variation of the skew angle at a fixed inclined angle of $\alpha=30$ deg and a typical hole length-to-diameter ratio of $L/D=3.5$.

2. Governing Equations

The governing equations for the steady Newtonian flow by using the Cartesian velocity component in a non-orthogonal coordinate were given as follows.

$$\frac{1}{j}\frac{\partial}{\partial x^j}[j\alpha_m^j(\rho U_m)]=0 \tag{1}$$

$$\frac{1}{j}\frac{\partial}{\partial x^j}[j\alpha_m^j(\rho U_m U_i-\tau_{mi}+P\delta_m^i)]=0 \tag{2}$$

$$\frac{1}{j}\frac{\partial}{\partial x^j}\left[j\alpha_m^j\left(\rho U_m T-\Gamma_{eff}\frac{\partial T}{\partial x^n}\right)\right]=0 \tag{3}$$

where

J : the Jacobian value of coordinate transformation

τ_{mi} : the Reynolds shear stress

α_m^j : the scalar product e^j and i_m

The turbulent viscosity for the standard $k-\varepsilon$ model was given by

$$\mu_t=\rho C_\mu\frac{k^2}{\varepsilon} \tag{4}$$

The transport equations of k and ε were given by

$$\frac{1}{J}\frac{\partial}{\partial x^j}\left[J\alpha_m^j\left(\rho U_m k-\frac{\mu_t}{\sigma_k}\frac{\partial k}{\partial x^n}\alpha_m^n\right)\right]=P_k-\rho\varepsilon \tag{5}$$

$$\frac{1}{J}\frac{\partial}{\partial x^j}\left[J\alpha_m^j\left(\rho U_m\varepsilon-\frac{\mu_t}{\sigma_\varepsilon}\frac{\partial\varepsilon}{\partial x^n}\alpha_m^n\right)\right]=\frac{\varepsilon}{k}\cdot(C_1P_k-C_2\rho\varepsilon) \tag{6}$$

$$P_k=\mu_t\left(\frac{\partial U_i}{\partial x^n}\alpha_j^n+\frac{\partial U_j}{\partial x^m}\alpha_i^m\right)\left(\frac{\partial U_i}{\partial x^n}\alpha_j^n\right)-\frac{2}{3}\left(\rho k+\mu_t\frac{\partial U_k}{\partial y^k}\right)\left(\frac{\partial U_k}{\partial y^k}\right) \tag{7}$$

The turbulence model constants used in the standard $k-\varepsilon$ model were given in Table 1.

3. Numerical Analysis

A non-orthogonal and non-uniform $80\times53\times46$ grid system was used to analyze the film cooling system injected through a hole with the inclined and skew angle and the variables were arranged as non-staggered. The plenum, hole and cross-stream region as shown in Fig. 2 were involved in the computational domain to get the realistic flow characteristics. The algebraic method using the interpolation function was used to generate the finer grid system near the wall.

The governing equations were discretized by a finite volume method. The power-law scheme for the convection term discretization and the central differencing scheme for the diffusion term were adapted.

The SIMPLE algorithm was used for pressure-velocity correction. The modified Rhie's method (Rhie, 1981) was used for pressure-velocity cou-

Table 1 $k-\varepsilon$ turbulence model constants.

Constants	σ_k	σ_ε	C_μ	C_1	C_2
Values	1.0	1.3	0.09	1.44	1.92

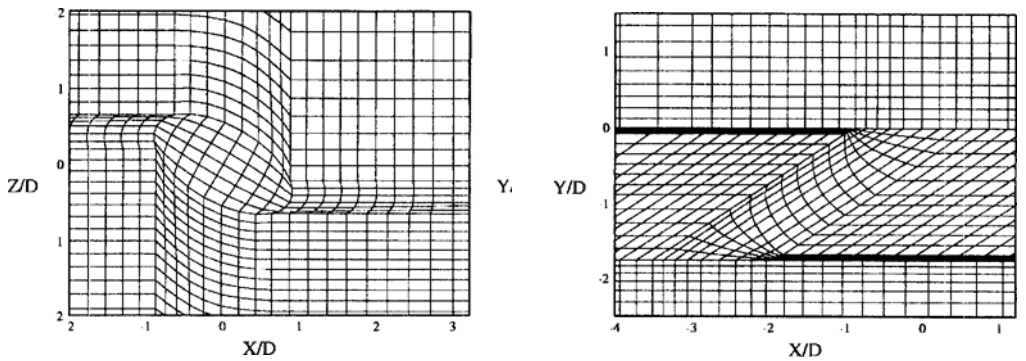

(a) Hole exit plane (b) Within the hole.

Fig. 2 Grid arrangement in the case of $\alpha=30$ deg and $\beta=30$ deg.

pling for the non-staggered grid. The disretization equations were solved by Strongly Implicit Procedure.

The inlet average velocity of the mainstream with the boundary layer thickness of $\delta=0.5833D$ based on the experimental data was 15 m/s and also the uniform velocity profile at the plenum inlet was imposed for the desired blowing ratio. The uniform inlet temperatures of the mainstream and plenum region were 320K and 300K respectively. The inlet conditions of the turbulent kinetic energy and energy dissipation rates were obtained from Eqs. (8) and (9) and the turbulence intensity TI was 0.5%.

$$k_{in}=(TI\cdot U_j)^2 \tag{8}$$

$$\varepsilon_{in}=\frac{C_\mu k_{in}^{3/2}}{0.1L_c} \tag{9}$$

At the symmetric plane, the normal gradients of all variables were prescribed as zero.

$$\frac{\partial\phi}{\partial n}=0 \tag{10}$$

The no-slip boundary condition was used at the wall and the adiabatic condition was implemented.

For the standard $k-\varepsilon$ model, the traditional wall function was applied and the wall shear stress for $y^+>11.63$ was obtained from the following equations.

$$y^+=\frac{\rho C_\mu^{1/4}k_P^{1/2}\delta_n}{\mu} \tag{11}$$

$$\tau_w=\frac{\rho_P C_\mu^{1/4}k_P^{1/2}\chi}{\ln(Ey_P^+)} \tag{12}$$

where $\chi=0.41$, $E=0.09$

4. Results and Discussion

In this study, the non-dimensional total pressure loss coefficient ($C_{P,inj}$), longitudinal vorticity (Q_X), longitudinal skin friction coefficient (C_{fX}), lateral skin friction coefficient(C_{fZ}) and the film cooling effectiveness(η) were calculated for $L/D=3.5$ and $\alpha=30°$. These parameters were defined as follows.

$$C_{P,inj}=\frac{P_\infty-P_{inj}}{\frac{1}{2}\rho U_\infty^2},\quad \Omega_X=\frac{D}{U_\infty}\left(\frac{\partial W}{\partial Y}-\frac{\partial V}{\partial Z}\right)$$

$$C_{fX}=\frac{\tau_{wX}}{\frac{1}{2}\rho U_\infty^2}=\frac{\mu\frac{\partial U}{\partial Z}}{\frac{1}{2}\rho U_\infty^2},$$

$$C_{fZ}=\frac{\tau_{wZ}}{\frac{1}{2}\rho U_\infty^2}=\frac{\mu\left.\frac{\partial W}{\partial Z}\right|_w}{\frac{1}{2}\rho U_\infty^2},\quad \eta=\frac{T_{ad}-T_j}{T_\infty-T_j}$$

where P_∞, U_∞ and T_∞ are the total pressure, velocity and temperature in the freestream region of the mainflow at $X/D=-10$. T_{ad} and T_j are the adiabatic wall temperature and the coolant temperature, respectively.

4.1 Comparison between prediction and Experiment

To validate the numerical results, the calculation was performed in the case that the jet was injected in the mainflow direction with the inclined angle of $\alpha=35$ deg and compared with the experimental results of Goldstein et al. (1970). Figure 3 shows the film cooling effectiveness along the center line with the blowing ratios of $M=0.5$, 1.0 and 2.0. The film cooling effectiveness shows an abrupt reduction near the hole and subsequent slow decrease in the downstream region, and it also shows a sudden reduction with increment of the blowing ratio. These results shows a fairly good agreement with the experimental data. Meanwhile, they show a large discrepancy near the hole. This results suggest that an improved turbulence modeling should be required for the near-hole region.

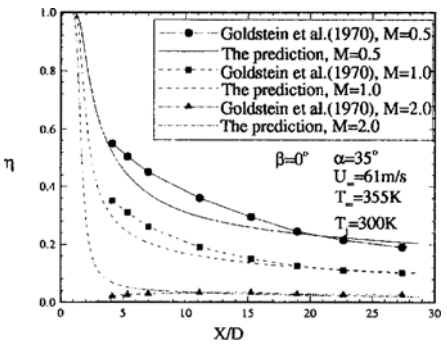

Fig. 3 Film cooling effectiveness along the center line for the blowing ratios of $M=0.5$, 1.0 and 2.0 at the inclined angle of $\alpha=35$ deg.

4.2 The effect of the skew angle

Figures 4 and 5 show the velocity distributions in the $Y-Z$ plane with the skew angle of $\beta=0$ deg and 60 deg. As shown in Fig. 4, a pair of counter-rotating vortices are formed and the center of those moves in the positive Y-direction by 0.5 D. This result shows the stronger diffusion into the normal direction than into the lateral direction. With the increase in the skew angle as in Fig. 5, the clockwise vortex is engulfed by the counter-clockwise vortex. Eventually only one strong counter-clockwise vortex remains in the downstream area. The center of this vortex moves towards the positive Z-direction by 0.7D. Consequently, the effective film cooling zone might be largely expanded in the Z-direction in the case of $\beta=60$ deg.

Figure 6 shows the contours of the total pressure loss coefficient $C_{P,inj}$ in the $Y-Z$ plane with the skew angles of $\beta=60$ deg and 90 deg. As shown in Fig. 6(a), the maximum total pressure loss coefficient appears near the wall. This is because the mainflow is the most effectively blockes by the jet flow in the region. As the skew angle increases as in Fig. 6(b), the aerodynamic loss became large due to the strong collision between the mainstream and injected jet, and the maximum total pressure loss appears at the center of the vortex as well as near the wall.

Figure 7 shows the longitudinal vorticity Ω_X distribution in the $Y-Z$ plane with the skew angles from $\beta=15$ deg to 90 deg. A pair of asymmetric vortices with different signs are formed in the case of $\beta=15$ deg and the counter-clockwise vortex has become much stronger than the clockwise vortex with the increase in the skew angle. The stronger vortex would engulf the weaker one and eventually formed a single vortex in the cases of $\beta=30$ deg and above. The maximum value of the vorticity increases with the

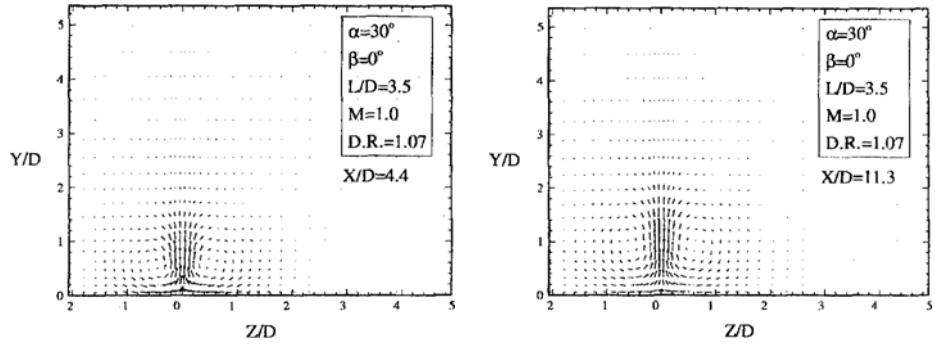

(a) $X/D=4.4$ (b) $X/D=11.3$

Fig. 4 Velocity distributions in the $Y-Z$ plane for $\beta=0$ deg.

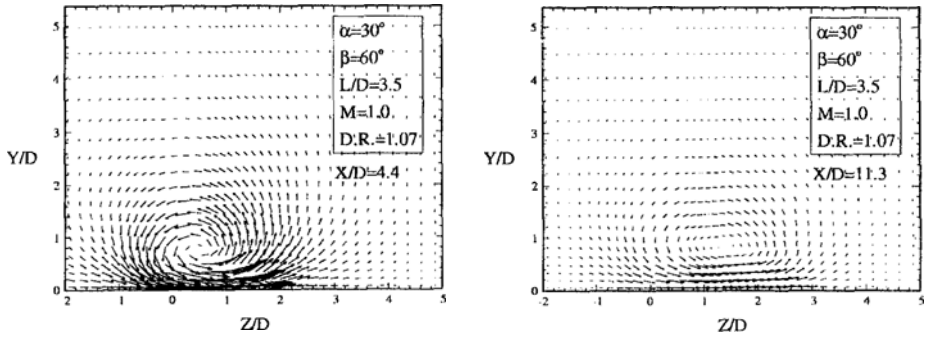

(a) $X/D=4.4$ (b) $X/D=11.3$

Fig. 5 Velocity distributions in the $Y-Z$ plane for $\beta=60$ deg.

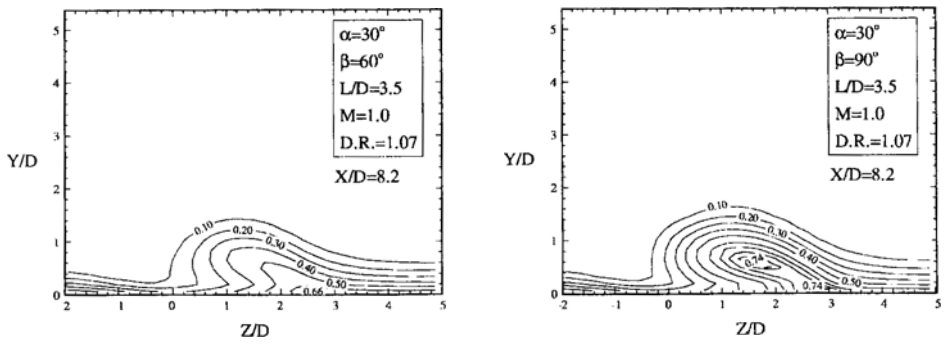

(a) $\beta=60$ deg (b) $\beta=90$ deg

Fig. 6 Contours of total pressure loss coefficients $C_{P,inj}$ in the $Y-Z$ plane with the skew angle.

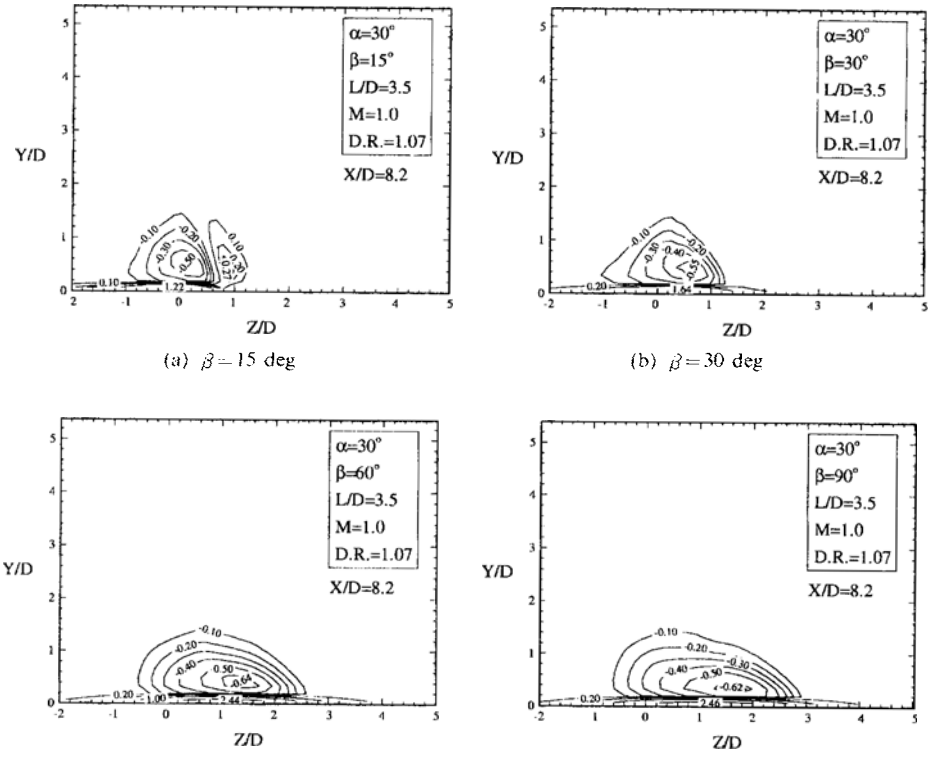

(a) $\beta=15$ deg (b) $\beta=30$ deg

(c) $\beta=60$ deg (d) $\beta=90$ deg

Fig. 7 Contours of longitudinal vorticity Ω_X in the $Y-Z$ plane with the skew angle.

increment of the skew angle, although it slightly decreases above $\beta=60$ deg. This trend shows good agreement with the results of Lee et al. (1997) and Compton and Johnston (1992).

Figure 8 shows the profiles of the longitudinal skin friction in the case of $\beta=0$ deg and 60 deg. For $\beta=0$ deg shown in Fig. 8(a), the distribution is symmetric distribution due to the presence of a pair of symmetric counter-rotating vortices. Due to the injected jet and the counter-rotating vortices, the mainstream velocity in the center plane $(Z/D=0)$ decreases and shows the minimum skin friction. As the vortex moves downstream, the skin friction coefficient slightly decreases due to diffusion of the vortex. In the case of $\beta=60$ deg shown in Fig. 8(b), asymmetric vortices shows quite different tendency. The stronger vortex survives and the maximum skin friction appears on

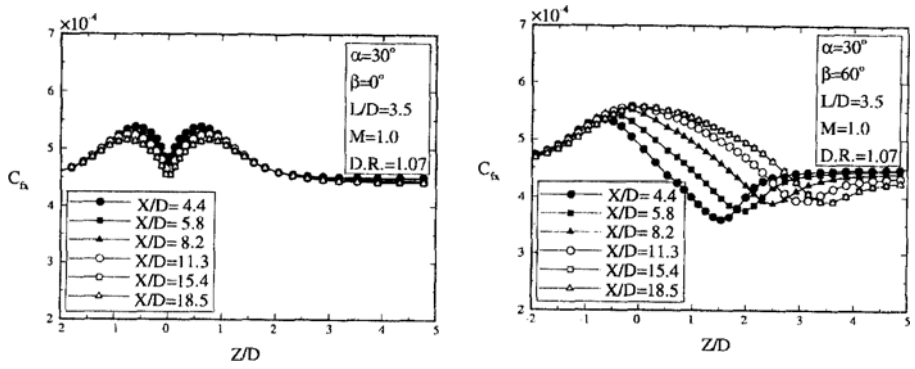

(a) $\beta=0$ deg (b) $\beta=60$ deg

Fig. 8 Profiles of longitudinal skin friction coefficient with the variation of the skew angle.

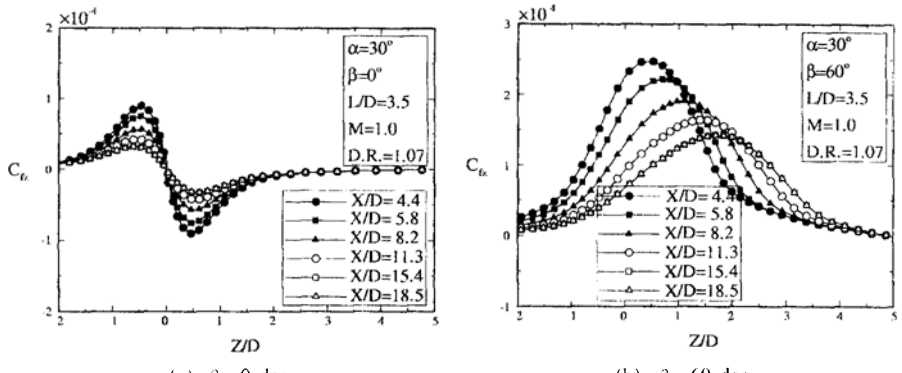

(a) $\beta=0$ deg (b) $\beta=60$ deg

Fig. 9 Profiles of lateral skin friction coefficient with the variation of the skew angle.

the left side of the vortex due to the high kinetic energy swept to the near-wall region by vortical motion and the minimum value appears on the right side due to the stagnant fluid with X-directional momentum decreases. This result shows the same tendency with the results of Zhang et al. (1993). As the vortex moves in the mainstream direction, the minimum value of the skin friction remains constant along the right side of the vortex.

Figure 9 shows the profiles of the lateral skin friction for $\beta=0$ deg and 60 deg. In the case of $\beta=0$ deg as shown in Fig. 9(a), the symmetric distributions with different signs are obtained due to the presence of a pair of symmetric counter-rotating vortices. The negative values of the lateral skin friction disappears in the case of $\beta=60$ deg. As the vortex moves downstream, the maximum value become smaller and shifted to the positive Z-direction.

Figure 10 shows the film cooling effectiveness distribution along the X-direction for $\beta=0$ deg and 60 deg. As shown in Fig. 10(a), the symmetric distribution is obtained in the case of $\beta=0$ deg and the maximum value appears in the center plane($Z/D=0$) where the skin friction is the minimum. The film cooling effectiveness decreases suddenly along the lateral direction due to the entrained mainstream. In the case of $\beta=60$ deg, the maximum value of the film cooling effectiveness is obtained on the right side of the vortex due to the stagnant fluid cumulating on this side.

4.3 The effect of hole length-to-diameter

In this study, to investigate the effect of L/D at jet exit, the flow fields within a film hole were numerically calculated with the variation of L/D

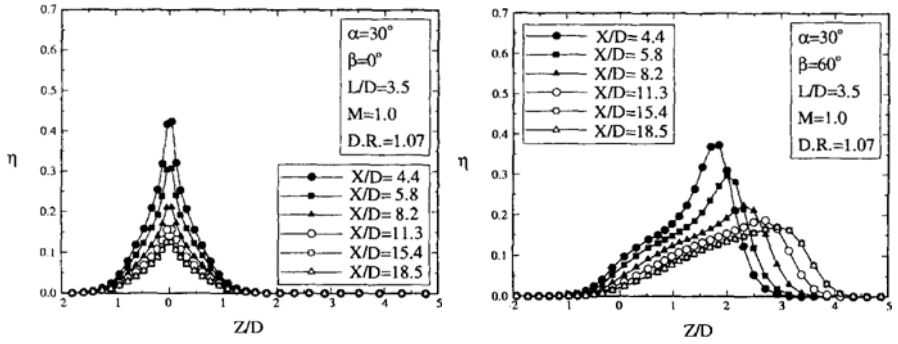

(a) $\beta=0°$ (b) $\beta=60°$

Fig. 10 Profiles of film cooling effectiveness with the variation of the skew angle.

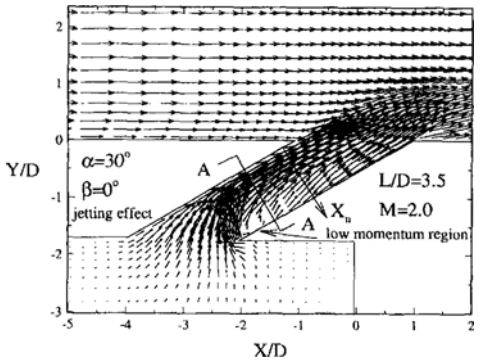

Fig. 11 Velocity distributions within film hole on the centerline plane.

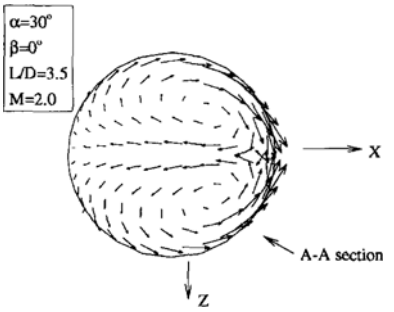

Fig. 12 Velocity distributions within the film hole on a plane perpendicular to the main flow direction(A-A section area of Fig. 11).

in the case of $M=2.0$ for $\alpha=30$ deg and $\beta=0$ deg.

Figures 11 and 12 shows the velocity distributions in the centerline plane and the plane perpendicular (A-A section) to the jet flow direction of the film hole for $L/D=3.5$. A low-momentum region in Fig. 11 appears near the inlet and downstream wall of the film hole and a strong jetting effect appears near the upstream wall as shown by Leylek and Zerkle(1994). As shown in Fig. 12 a pair of counter-rotating vortices were also formed. Leylek and Zerkle(1994) showed that the velocity profiles of coolant jets in the jet exit plane were controlled by the combination of three mechanisms; relative magnitude of main flow and coolant jet momentum, strength of jetting effect near upstream wall and strength of counterrotating vortex structure.

Figure 13 shows the non-dimensional jet velocity profiles at the jet exit with the variation of L/D. For $L/D=3.5$, the peak of the jet velocity appears in the upstream region of the jet exit plane. Most of the coolant jet flow exits through the upstream region of the jet exit plane. This is because the coolant jet momentum(i. e. jetting effect) is much stronger than mainflow momentum. The jet velocity profile in the case of $L/D=7.0$ is similar to that in the case of $L/D=3.5$.

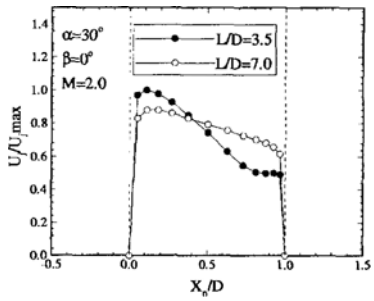

Fig. 13 Non-dimensional jet velocity profiles at the jet exit.

However, the jet velocity in the upstream region of the jet exit plane decreases and the jet velocity in the downstream region increases in comparison with that for $L/D=3.5$. This is caused by a decrease in the jetting effect due to the decrease in the cooling jet momentum at the jet exit with the increment of L/D.

5. Conclusion

In the present study, flow and heat transfer characteristics were numerically calculated from the three-dimensional Navier-Stokes equations to understand the effect of the skew angle($\beta=0 \sim 90$ deg) on the film-cooling performance. The following conclusions were obtained.

(1) The maximum total pressure loss coefficient appears near the wall for $\beta=0$ deg. As the skew angle increases, the aerodynamic loss become large and the injected jet and the maximum total pressure loss appears at the center of the vortex as well as near the wall.

(2) For $\beta=0$ deg, the minimum skin friction is shown in the center plane($Z/D=0$). As the vortex moves downstream, the skin coefficient slightly decreass. For $\beta=60$ deg, the maximum skin friction appears on the left side of the vortex and the minimum value appears on the right side. As the vortex moves along the mainstream direction, the minimum value of the skin friction remains constant along the right side of the vortex.

(3) For $\beta=0$ deg, the maximum value of the film cooling effectiveness appears in the center plane($Z/D=0$). For $\beta=60$ deg, the maximum value of the film cooling effectiveness is obtained on the right side of the vortex.

(4) The jet velocity in the upstream region of the jet exit plane decreass with the increment of L/D. On the other hand, the jet velocity in the downstream region increases.

Acknowledgements

This research was supported by 1997 Chung Ang University Research Fund and partially supported by the Turbo and Power Machinery Research Center.

References

Compton, D. A. and Johnston, J. P., 1992, "Streamwise Vortex Production by Pitched and Skewed Jets in a Turbulent Boundary Layer," *AIAA Journal,* Vol. 30, No. 3, pp. 640~ 647.

Goldstein, R. J., Eckert, E. R. G., and Ramsey, J. W., 1970, "Film Cooling Following Inj ection Through Inclined Circular Tubes," *Israel Journal of Technology,* Vol. 8, pp. 584-588.

Honami, S., Shizawa, T. and Uchiyama, A., 1994, "Behavior of the Laterally Injected Jet in Film Cooling: Measurements of Surface Temperature and Velocity Temperature Field within the Jet," *ASME J. of Turbomachinery,* Vol. 116, pp. 106~112.

Lee, S. W., Kim, Y. B. and Lee, J. S., 1997, "Flow Characteristics and Aerodynamic Losses of Film-Cooling Jets with Compound Angle Orientations," *ASME J. of Turbomachinery,* Vol. 119, pp. 310~319.

Leylek, J. H. and Zerkle, R. D., 1994, "Discrete-Jet Film Cooling: A Comparison of Computational Results with Experiments," *ASME J. of Turbomachinery,* Vol. 116, pp. 358~368.

Ligrani, P. M. and Mitchell, S. W., 1994, "Interactions Between Embedded Vortices and Injectant from Film Cooling Holes with Compound Angle Orientations in a Turbulent Boundary Layer," *ASME J. of Turbomachinery,* Vol. 116, pp. 709~720.

Rhie, C. M., 1981, "A Numerical Study of the Flow Past an Isolated Airfoil with Separation," Ph. D. Thesis, Dept. of Mech., University of Illinois at Urbana-Champagn.

Sinha, A. K., Bogard, D. G. and Crawford, M. E., 1991, "Film Cooling Effectiveness Downstream of a Single Row of Holes with Variable Density Ratio," *ASME J. of Turbomachinery,* Vol. 113, pp. 442~449.

Zhang, X. and Collins, M. W., 1993, "Flow and Heat Transfer in a Turbulent Boundary Layer Through Skewed and Pitched Jets," *AIAA Journal,* Vol. 31, No. 9, pp. 1590~ 1599.